Transient Pressure Analysis for Fractured Wells

Heber Cinco-Ley,* SPE, Stanford U.
Fernando Samaniego-V.,* SPE, Inst. Mexicano del Petróleo

7490

Summary

A new technique is presented for analyzing pressure transient data for wells intercepted by a finite-conductivity vertical fracture. This method is based on the bilinear flow theory, which considers transient linear flow in both fracture and formation. It is demonstrated that a graph of p_{wf} vs. $t^{1/4}$ produces a straight line whose slope is inversely proportional to $h_f(k_f b_f)^{1/2}$. New type curves are presented that overcome the uniqueness problem exhibited by other type curves.

Introduction

A large amount of information concerning well test analysis has appeared in the literature over the last three decades. As a result of developments in this area, three monographs[1,2,3] and one book[4] have been published covering different aspects of pressure transient analysis. Ramey[5] also has presented a review on the state of the art.

The analysis of pressure data for fractured wells has deserved special attention because of the number of wells that have been stimulated by hydraulic fracturing techniques. A summary of the work done on flow toward fractured wells was presented by Raghavan[6] in 1977.

It was recognized early that intercepting fractures can strongly affect the transient flow behavior of a well[7-9] and that, consequently, the application of classical methods[10-12] to the analysis of transient pressure data in this situation may produce erroneous results. Several methods[13-24] were proposed to solve this problem.

These analysis techniques consider a well intersected by either an infinite-conductivity vertical fracture or a uniform-flux vertical fracture. Cinco-Ley *et al.*[25] demonstrated that the assumption of infinite fracture conductivity is valid whenever the dimensionless fracture conductivity $(k_f b_f / k x_f) \geq 300$; all other cases, such as those represented by long or poorly conductive fractures, must be analyzed by considering a finite-conductivity fracture model.

Exploitation of low-permeability gas reservoirs has required stimulation of wells by massive hydraulic fracturing (MHF) techniques. Vertical fractures of large horizontal extension are created as a result of this operation; consequently, pressure drop along the fracture cannot be neglected.

Several papers[25-32] have been published on the behavior of finite-conductivity vertical fractures. Type-curve matching has been proposed as an analysis method under these conditions; however, some regions of the curves present a uniqueness problem in the analysis. Barker and Ramey[31] indicated that the use of published type curves becomes practical when a large span of pressure data is available.

The purpose of this work is to present a new interpretation technique for early-time pressure data for a well intercepted by a finite-conductivity vertical fracture, including the criteria to determine the end of wellbore storage effects. In addition, new type curves are discussed to overcome the uniqueness problem exhibited by previous curves at intermediate and large time values.

Transient Pressure Behavior for Fractured Wells

Consider a vertically fractured well producing at a constant flow rate, q, in an infinite, isotropic, homogeneous, horizontal reservoir that contains a slightly compressible fluid of constant compressibility c, and viscosity μ. The porous medium has a permeability k, porosity ϕ, thickness h, and initial pressure p_i.

Let us assume that the well is intercepted by an undeformable, fully penetrating vertical fracture of

*Now with Petróleos Mexicanos and U. Nacional de Mexico.

0149-2136/81/0009-7490$00.25

TABLE 1 – SI PREFERRED UNITS, CUSTOMARY UNITS, AND UNIT CONVERSION CONSTANTS USED IN THESE SYSTEMS

Parameter or Variable	SI Preferred Units	Customary Units
k	μm^2	md
h	m	ft
q_o	m^3/d	STB/D
q_g	m^3/d	Mscf/D
μ	Pa·s	cp
B	m^3/m^3	RB/STB
ϕ	fraction	fraction
c_t	Pa^{-1}	psi^{-1}
p	kPa	psi
$m(p)$	$kPa^2/Pa \cdot s$	psi^2/cp
t	hours	hours
α_o	1,842	141.2
α_g	1,293	1,424
β	3.6×10^{-9}	2.637×10^{-4}
δ_{bfo}	34.97	44.1
δ_{bfg}	24.57	444.75
δ_{lfo}	0.3918	8.128
δ_{lfg}	0.275	81.97
T	K	°R
C	m^3/Pa	cu ft/psi

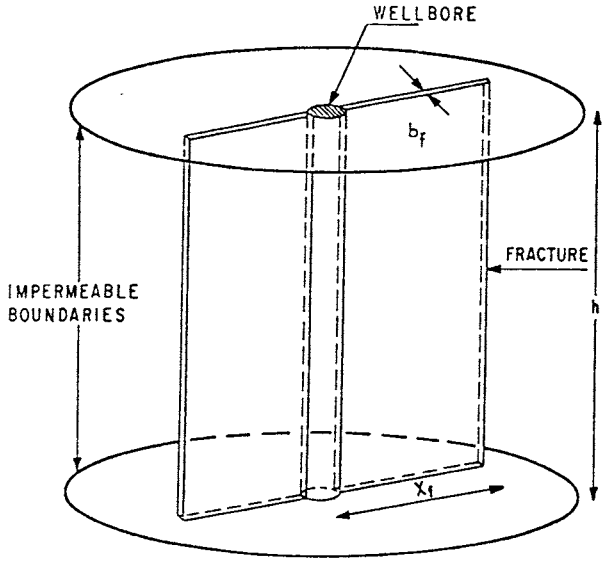

Fig. 1 – Finite-conductivity vertical fracture in an infinite-slab reservoir.

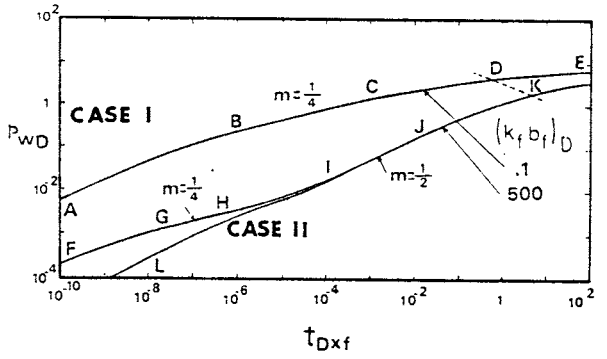

Fig. 2 – Low-log graph of typical cases for fractured wells.

half-length x_f, width b_f, permeability k_f, porosity ϕ_f, and total compressibility c_{ft} (Fig. 1). The properties of both the reservoir and the fracture are independent of pressure and the flow in the entire system obeys Darcy's law. In addition, it is convenient to assume that pressure gradients are small, gravity effects are negligible, and flow entering the wellbore comes only through the fracture.

With these assumptions, the unsteady-state flow in the system can be described by the diffusivity equation.[1] For details on the boundary conditions and a semianalytical solution for this flow problem, see Ref. 25.

The general solution for the wellbore flowing pressure p_{wf} for oil is given by[25]

$$\frac{kh(p_i - p_{wf})}{\alpha_o q B \mu} = p_{wD}(t_{Dx_f}, \eta_{fD}, C_{fDf}) \quad \ldots\ldots (1)$$

and, for gas,

$$\frac{kh[m(p_i) - m(p_{wf})]}{\alpha_g q T} = p_{wD}(t_{Dx_f}, \eta_{fD}, C_{fDf}), \quad \ldots\ldots (2)$$

where

$$t_{Dx_f} = \frac{\beta k t}{\phi \mu c_t x_f^2}, \quad \ldots\ldots (3)$$

$$\eta_{fD} = \frac{k_f \phi c_t}{k \phi_f c_{ft}}, \quad \ldots\ldots (4)$$

and

$$C_{fDf} = \frac{b_f \phi_f c_{ft}}{\pi x_f \phi c_t}. \quad \ldots\ldots (5)$$

p_{wD} represents the dimensionless pressure drop; it is a function of dimensionless time, t_{Dx_f}, dimensionless fracture hydraulic diffusivity, η_{fD}, and dimensionless fracture storage capacity, C_{fDf}. α_o, α_g, and β are unit conversion constants (see Table 1).

Cinco-Ley *et al.*[25] showed that for practical values of dimensionless time the pressure behavior depends on two parameters only: the dimensionless time t_{Dx_f}, and the dimensionless fracture conductivity $(k_f b_f)_D$. The former was defined in Eq. 3 and the latter may be obtained from Eqs. 4 and 5. By definition, the dimensionless fracture conductivity is

$$(k_f b_f)_D = \frac{k_f b_f}{k x_f}, \quad \ldots\ldots (6)$$

and it appears to be related to C_{fDf} and η_{fD} as follows.

$$(k_f b_f)_D = \pi C_{fDf} \eta_{fD}. \quad \ldots\ldots (7)$$

Fig. 2 shows the general behavior of a well with a finite-conductivity vertical fracture. There, we show a log-log graph of dimensionless wellbore pressure, p_{wD}, vs. dimensionless time, t_{Dx_f}. For the sake of simplicity only two cases are presented. Case 1 represents the behavior of a low-conductivity

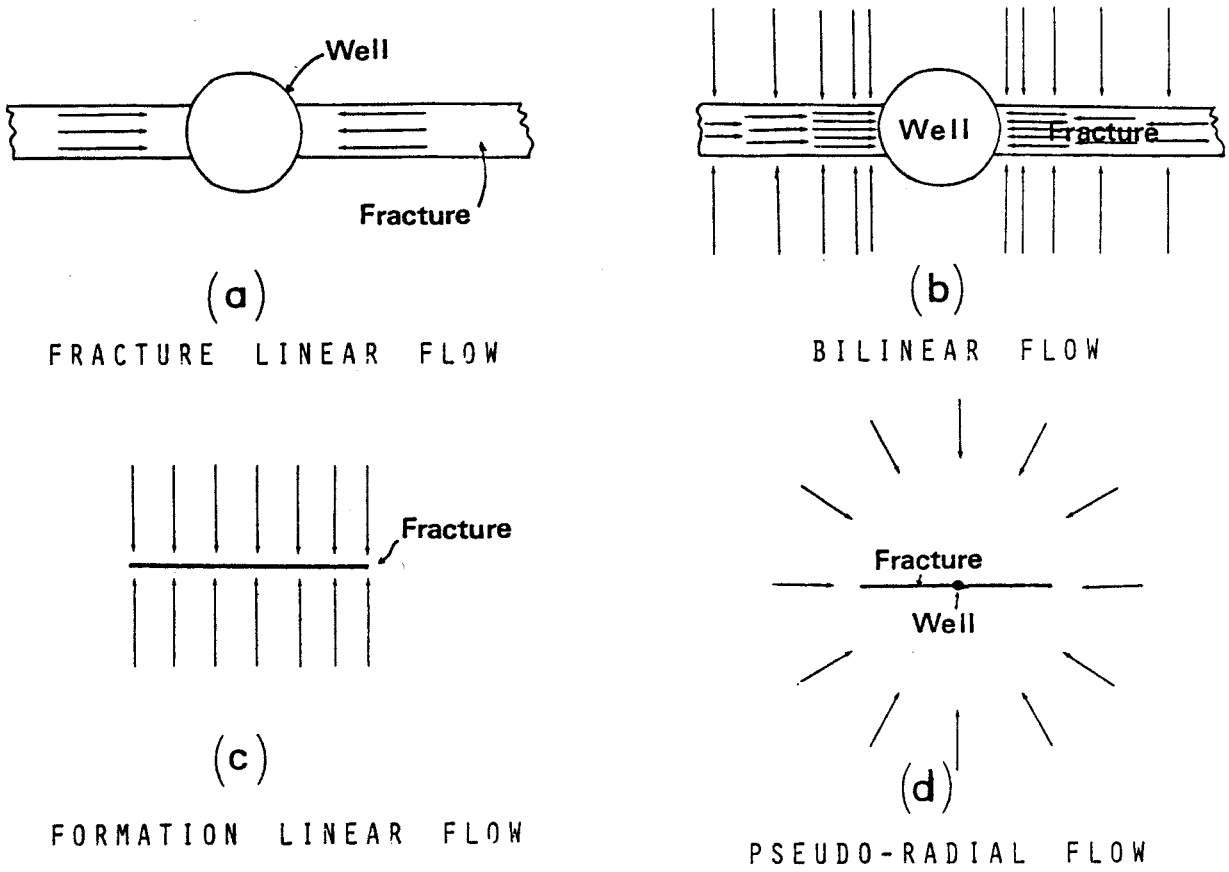

Fig. 3 – Flow periods for a vertically fractured well.

fracture $(k_f b_f)_D = 0.1$; Case 2 considers a highly conductive fracture, $(k_f b_f)_D = 500$. These cases were selected because they exhibit all the features of the transient pressure behavior for a fractured well.

An analysis of Fig. 2 shows that the transient behavior of a well with a finite-conductivity vertical fracture includes several flow periods. Initially, there is a *fracture* linear flow characterized by a half-slope straight line; after a transition flow period, the system may or may not exhibit a *bilinear flow period*, indicated by a one-fourth-slope straight line. As time increases, a formation linear flow period might develop. Eventually, in all cases, the system reaches a pseudoradial flow period (see Fig. 3).

Points A, F, and L in Fig. 2 represent the end of the fracture linear flow period (half-slope straight line). The bilinear flow period (one-quarter-slope straight line) is defined by Segments B-C and G-H; this behavior is not present when the fracture has a high storage capacity and a high conductivity (lower curve in Case 2).

The formation linear flow period is shown by the half-slope straight line between Points I and J, and it is only exhibited by fractures of high conductivity, $(k_f b_f)_D \geq 300$. Points D and K show the beginning of the pseudoradial flow period.

We present a detailed description of both the fractured linear flow and the bilinear flow. The formation linear flow and the pseudoradial flow have been discussed in the literature.[14,15,17,19,22,25]

Fracture Linear Flow Period

This behavior occurs at very small values of dimensionless time, and it is exhibited by all cases. During this flow period, most of the fluid entering the wellbore comes from the expansion of the system within the fracture and the flow is essentially linear, as shown in Fig. 3a.

The dimensionless pressure response at the wellbore is given by*

$$p_{wD} = \frac{2}{(k_f b_f)_D} \sqrt{\pi \eta_{fD} t_{Dx_f}} \quad \ldots\ldots\ldots\ldots (8)$$

Hence, for oil,

$$p_{wf} = p_i - \frac{\delta_{tfo} qB}{b_f h} \sqrt{\frac{\mu t}{k_f \phi_f c_{ft}}}, \quad \ldots\ldots\ldots\ldots (9)$$

and for gas,

$$m(p_{wf}) = m(p_i) - \frac{\delta_{tfg} qT}{b_f h} \sqrt{\frac{t}{k_f \phi_f \mu c_t}}, \quad \ldots\ldots (10)$$

where δ_{tfo} and δ_{tfg} are unit conversion constants.

These equations indicate that a log-log graph of pressure vs. time yields a straight line whose slope is equal to one half. A graph of pressure or pseudopressure vs. the square root of time also gives a straight line whose slope depends on the fracture characteristics excluding the fracture half-length x_f.

The fracture linear flow ends when

*See Appendix A for derivation.

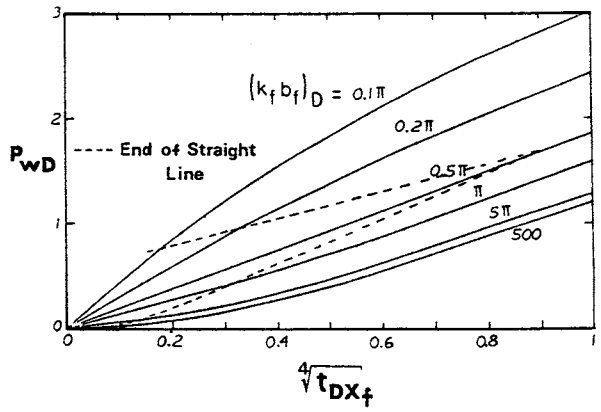

Fig. 4 – p_{wD} vs. $t_{Dx_f}^{1/4}$ for a well with a finite-conductivity vertical fracture.

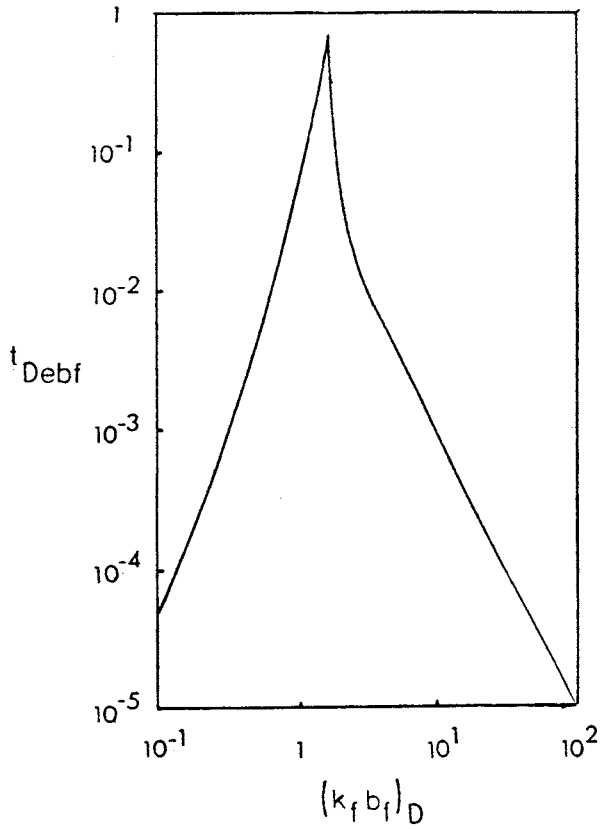

Fig. 5 – Dimensionless time for the end of the bilinear flow period vs. dimensionless fracture conductivity.

$$t_{Dx_f} \simeq \frac{0.01(k_f b_f)_D^2}{\eta_{fD}^2}. \quad \ldots\ldots\ldots\ldots\ldots\ldots (11)$$

Unfortunately, this flow period occurs at a time too early to be of practical use.

Bilinear Flow Period

To the best of our knowledge, this is a new type of flow behavior that has not been considered in the literature. It is called bilinear flow because two linear flows occur simultaneously. One flow is a *linear incompressible flow* within the *fracture* and the other is a *linear compressible flow* in the *formation*, as shown in Fig. 3b. A bilinear flow exists, as shown in Appendix A, whenever most of the fluid entering the wellbore comes from the formation and fracture tip effects have not yet affected the well behavior.

Let us now examine this behavior in a log-log graph of p_{wD} vs. t_{Dx_f} (Fig. 2). In Case 1 $[(k_f b_f)_D = 0.1]$, the bilinear flow exists between Points B and C after a transition flow period represented by Segment A-B. The pressure behavior for the *bilinear flow* exhibits a *straight line* whose *slope* is equal to *one fourth*. The duration of this period depends on both $(k_f b_f)_D$ and C_{fDf}. Case 2 $[(k_f b_f)_D = 500]$ may or may not exhibit the bilinear flow period, as shown by the upper and lower curves. The upper curve for Case 2 corresponds to a low value for C_{fDf} and does exhibit bilinear flow over a short period of time (Segment G-H); however, the lower curve corresponding to a high value of C_{fDf} does not exhibit the bilinear flow behavior because fracture tip effects are felt before this flow regime is established (Segment L-I).

The dimensionless wellbore pressure for the bilinear flow period is given by*

$$p_{wD} = \frac{\pi}{\Gamma(1.25)\sqrt{2(k_f b_f)_D}} t_{Dx_f}^{1/4}, \quad \ldots\ldots\ldots (12)$$

or

$$p_{wD} = \frac{2.45}{\sqrt{(k_f b_f)_D}} t_{Dx_f}^{1/4}. \quad \ldots\ldots\ldots\ldots\ldots (13)$$

This equation indicates that a graph of p_{wD} vs. $\sqrt[4]{t_{Dx_f}}$ produces a straight line whose slope is $2.45/\sqrt{(k_f b_f)_D}$, intercepting the origin. Fig. 4 presents that type of graph for different values of $(k_f b_f)_D$.

An important feature of this graph is that after the bilinear flow period (straight-line portion), the curves for $(k_f b_f)_D \leq 1.6$ are concave downward and the curves for $(k_f b_f)_D > 1.6$ are concave upward.

The end of the straight-line portion of the curves depends on the fracture conductivity and may be expressed by

$$t_{Debf} \simeq \frac{0.1}{(k_f b_f)_D^2} \text{ for } (k_f b_f)_D \geq 3, \quad \ldots\ldots (14a)$$

*See Appendix A for derivation.

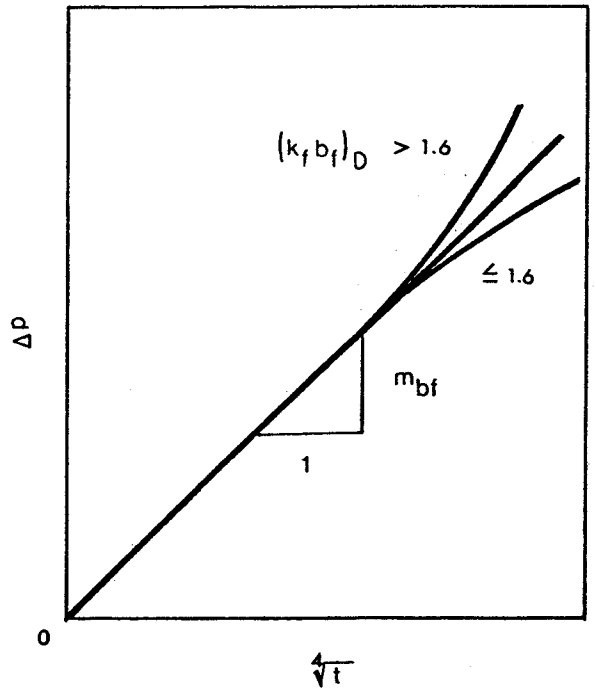

Fig. 6 – Graph for analysis of pressure data of bilinear flow.

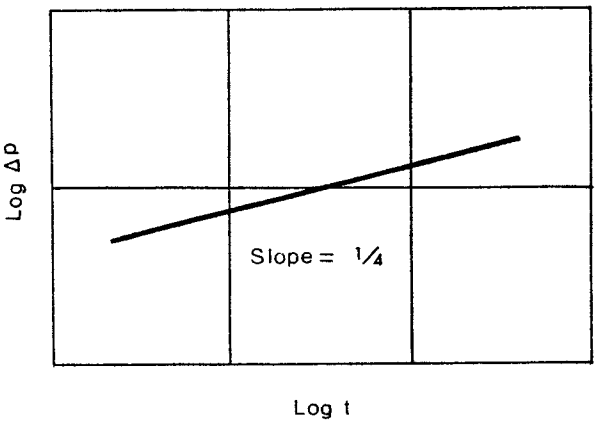

Fig. 7 – Log-log graph of pressure data for bilinear flow.

$$t_{Debf} \simeq 0.0205\left[(k_f b_f)_D - 1.5\right]^{-1.53}$$

$$\text{for } 1.6 \leq (k_f b_f)_D \leq 3, \quad \ldots\ldots\ldots\ldots (14b)$$

and

$$t_{Debf} \simeq \left[\frac{4.55}{\sqrt{(k_f b_f)_D}} - 2.5\right]^{-4}$$

$$\text{for } (k_f b_f)_D \leq 1.6. \quad \ldots\ldots\ldots\ldots\ldots (14c)$$

Fig. 5 shows a graphical representation of these equations.

Bilinear Flow Analysis

Bilinear flow is exhibited by finite-conductivity fractures with a small dimensionless storage capacity, C_{fDf}. Any attempt to analyze pressure data observed over this flow period using conventional methods (p vs. $\sqrt{t}$ or p vs. log t) will produce erroneous results. We present the appropriate analysis method based on the bilinear flow theory.

Basic Equations and Graphs

From Eq. 13, the pressure drop for oil may be expressed as

$$\Delta p = \frac{\delta_{bfo} qB\mu}{h(k_f b_f)^{1/2}(\phi\mu c_t k)^{1/4}} \sqrt[4]{t}, \quad \ldots\ldots\ldots\ldots (15)$$

and, for gas,

$$\Delta m(p) = \frac{\delta_{bfg} qT}{h(k_f b_f)^{1/2}(\phi\mu c_t k)^{1/4}} \sqrt[4]{t}, \quad \ldots\ldots\ldots (16)$$

where Δp is the pressure (pseudopressure) change for a given test. Both δ_{bfo} and δ_{bfg} are unit conversion constants and are given in Table 1.

Eqs. 15 and 16 indicate that the pressure change is both inversely proportional to the square root of the fracture conductivity and directly proportional to the fourth root of time.

According to Eqs. 15 and 16, a graph of Δp vs. $\sqrt[4]{t}$ produces a straight line passing through the origin, whose slope, m_{bf}, for oil, is given by

$$m_{bf} = \frac{\delta_{bfo} qB\mu}{h(k_f b_f)^{1/2}(\phi\mu c_t k)^{1/4}}, \quad \ldots\ldots\ldots\ldots (17)$$

and, for gas,

$$m_{bf} = \frac{\delta_{bfg} qT}{h(k_f b_f)^{1/2}(\phi\mu c_t k)^{1/4}}, \quad \ldots\ldots\ldots\ldots (18)$$

Hence, the product $h(k_f b_f)^{1/2}$ can be estimated by using the following equations. For oil,

$$h(k_f b_f)^{1/2} = \frac{\delta_{bfo} qB\mu}{m_{bf}(\phi\mu c_t k)^{1/4}}, \quad \ldots\ldots\ldots\ldots (19)$$

and, for gas,

$$h(k_f b_f)^{1/2} = \frac{\delta_{bfg} qT}{m_{bf}(\phi\mu c_t k)^{1/4}}. \quad \ldots\ldots\ldots\ldots (20)$$

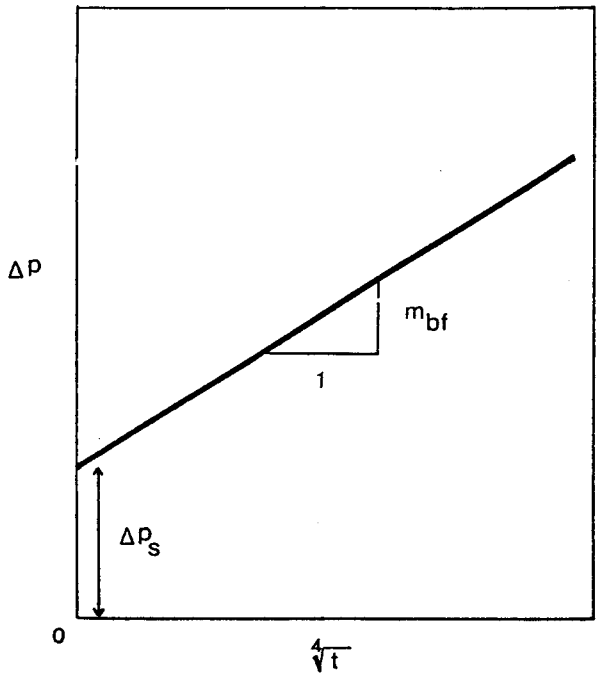

Fig. 8 – Bilinear-flow graph for a fracture with a flow restriction near the wellbore.

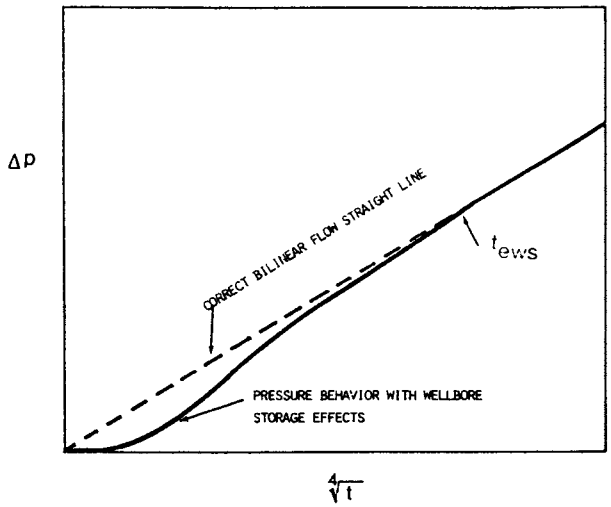

Fig. 9 – Wellbore storage effect on the bilinear flow graph.

These equations indicate that values of reservoir properties must be available to estimate the group $h(k_f b_f)^{1/2}$. Note that this analysis technique tends to decrease the effect of the error introduced when poor information on reservoir properties (i.e., k, ϕ, and c_t) is used.

All comments on the concavity of the curve in Fig. 4 are valid for the curve in Fig. 6.

From Eqs. 13 and 14, if $(k_f b_f)_D \geq 3$, the dimensionless pressure drop at the end of the bilinear flow period is given by

$$(p_{wD})_{ebf} \simeq \frac{1.38}{(k_f b_f)_D}. \quad \ldots\ldots\ldots\ldots\ldots\ldots (21)$$

Hence, the dimensionless fracture conductivity can be estimated using the following equation.

$$(k_f b_f)_D \simeq \frac{1.38}{(p_{wD})_{ebf}}. \quad \ldots\ldots\ldots\ldots\ldots\ldots (22)$$

$(p_{wD})_{ebf}$ can be calculated using Eq. 1 or Eq. 2 and $(\Delta p)_{ebf}$ or $\Delta m(p)_{ebf}$ obtained from the bilinear flow graph.

From Eqs. 15 and 16, a graph of log Δp vs. log t yields a quarter-slope straight line (Fig. 7) that can be used as a diagnostic tool for bilinear flow detection.

Extensions and Limitations

The region disturbed during bilinear flow includes only the fracture and its vicinities because it occurs at early time, even in partially penetrating fracture systems. Thus, the equations and graphs discussed in the previous section for bilinear flow can be extended to cases where the fracture does not penetrate the entire thickness of the formation. This is possible simply by using the fracture height, h_f, instead of the formation thickness, h.

In cases where a flow restriction (low conductivity, turbulent flow) exists within the fracture in the vicinity of the wellbore, bilinear flow still occurs and the pressure data analysis discussed can be applied (see Fig. 8). An extra pressure drop, Δp_s, is created in this case and the straight-line portion does not intercept the origin. These situations distort the straight-line portion in the log-log graph.

If wellbore storage affects the system, the bilinear flow pressure behavior may be masked, as shown in Fig. 9, and data analysis becomes difficult (if not impossible) with current interpretation methods.

Flow Regime Identification and New Type Curves

The pressure behavior of a fractured well may exhibit several flow periods for practical values of time: bilinear flow, formation linear flow, and pseudoradial flow.

Pressure data for each flow period should be analyzed using a specific interpretation method (i.e., p_w vs. $\sqrt[4]{t}$, p_w vs. $\sqrt{t}$, and p_w vs. log t for bilinear, linear, and pseudoradial flows, respectively).

The log-log graph has been used commonly as a diagnostic tool to detect different flow regimes in a transient pressure test. The use of type curves in the analysis of pressure data for fractured wells represents a major step in that area. The first type curves for fractured wells were presented by Gringarten *et. al.*[19] Cinco-Ley *et al.*[25] showed that the infinite-conductivity vertical fracture solution of Gringarten and Ramey[17] behaves like the solution

for a finite-conductivity vertical fracture of $(k_f b_f)_D \geq 300$; furthermore, they showed that the uniform-flux vertical fracture behaves as a variable-conductivity vertical fracture. The type-curve analysis offers an advantage over the specific analysis methods already mentioned because it can be applied to interpret at once pressure test data that correspond to different flow periods. In addition, the type-curve analysis could indicate when the different graphical techniques apply.

Experience has shown that, in some cases, application of the type curves available for finite-conductivity vertical fractures does not yield unique results. This is because the shape of pressure behavior curves is similar for different values of dimensionless fracture conductivity over some regions of the type curves. A close inspection of Fig. 2 indicates that the uniqueness problem can exist if pressure data to be analyzed occur at either the bilinear flow period (one-fourth slope) or the pseudoradial flow period.

A convenient presentation of the type curve published by Cinco-Ley *et al.*,[25] Ramey *et al.*,[31] and Agarwal *et al.*[29] is given in Fig. 10. We show a graph of log $[p_{wD}(k_f b_f)_D]$ vs. log $[t_{Dx_f}(k_f b_f)^2_D]$.* The main feature of this graph is that for all values of $(k_f b_f)_D$ the behavior of both bilinear flow (quarter slope) and the formation linear flow (half slope) is given by a single curve. Note that there is a transition period between the bilinear and linear flows. The dashed line in this figure indicates the approximate start of the pseudoradial flow period (semilog straight line). Also shown are the end of the bilinear flow and the start of the formation linear flow; the time for the end of the bilinear flow from Fig. 10 agrees with the results presented in Fig. 5. The groups of variables used in Fig. 10 were derived in Appendix B, where it is shown that, for some values of fracture conductivity, bilinear flow ends when fracture tip effects are felt at the wellbore.

Although many curves are presented for $(k_f b_f)_D > 20\pi$, the shape of these lines is essentially the same. The only difference is the duration of the formation linear flow (half slope); that is, the higher the fracture conductivity, the longer the linear flow period.

The beginning of the formation linear flow occurs at $t_{Dx_f}(k_f b_f)^2_D \approx 10^2$; that is,

$$t_{Dblf} \simeq \frac{100}{(k_f b_f)^2_D} \quad \ldots\ldots\ldots\ldots\ldots\ldots\ldots\ldots (23)$$

The end of this flow period is given by[19]

$$t_{Delf} \simeq 0.016. \quad \ldots\ldots\ldots\ldots\ldots\ldots\ldots\ldots (24)$$

Hence, the fracture conductivity may be estimated as follows:

$$(k_f b_f)_D \simeq \frac{10}{\sqrt{t_{Dblf}}}, \quad \ldots\ldots\ldots\ldots\ldots\ldots\ldots (25)$$

*A large-scale copy of this graph may be obtained from the authors.

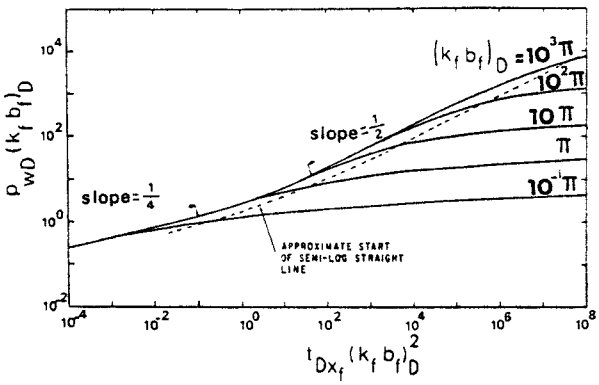

Fig. 10 – Type curve for vertically fractured wells.

or

$$(k_f b_f)_D \simeq 1.25 \times 10^{-2} \sqrt{\frac{t_{elf}}{t_{blf}}}. \quad \ldots\ldots\ldots\ldots (26)$$

These equations apply when $(k_f b_f)_D \geq 100$.

Fig. 10 can be used as a type curve to analyze pressure data for a fractured well. Pressure data on a graph of log Δp vs. log t is matched on a type curve to determine $(\Delta p)_M$, $[p_{wD}(k_f b_f)_D]_M$, $(t)_M$, $[t_{Dx_f} \cdot (k_f b_f)^2_D]_M$, $[(k_f b_f)_D]_M$, $(t_{ebf})_M$, $(t_{blf})_M$, and $(t_{bssl})_M$. From this information, we can estimate the following.

Dimensionless Fracture Conductivity.

$$\left[(k_f b_f)_D\right]_M$$

Formation Permeability. For oil,

$$k_o = \frac{\alpha_o q B \mu}{h(\Delta p)_M} \frac{[p_{wD} \cdot (k_f b_f)_D]_M}{[(k_f b_f)_D]_M}, \quad \ldots\ldots\ldots (27)$$

and, for gas,

$$k_g = \frac{\alpha_g q T}{h[\Delta m(p)]_M} \frac{[p_{wD} \cdot (k_f b_f)_D]_M}{[(k_f b_f)_D]_M}. \quad \ldots\ldots\ldots (28)$$

Fracture Half-Length.

$$x_f = \left[\frac{\beta k(t)_M}{\phi \mu c_t} \frac{[(k_f b_f)_D]^2_M}{[t_{Dx_f} \cdot (k_f b_f)^2_D]_M} \right]^{1/2}. \quad \ldots\ldots\ldots (29)$$

Fracture Conductivity.

$$k_f b_f = k x_f [(k_f b_f)_D]_M. \quad \ldots\ldots\ldots\ldots\ldots (30)$$

End of Bilinear Flow.

$$(t_{ebf})_M$$

Beginning of Formation Linear Flow.

$$(t_{blf})_M$$

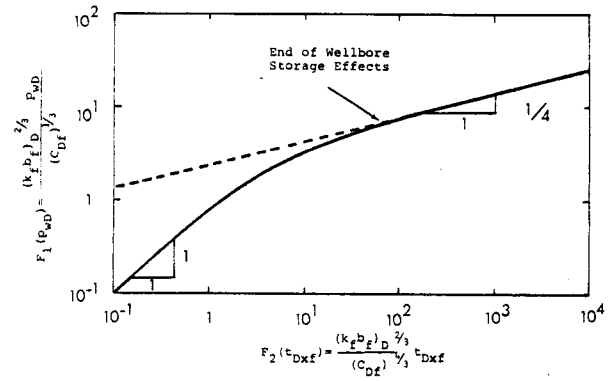

Fig. 11 – Type curve for wellbore storage under bilinear flow conditions.

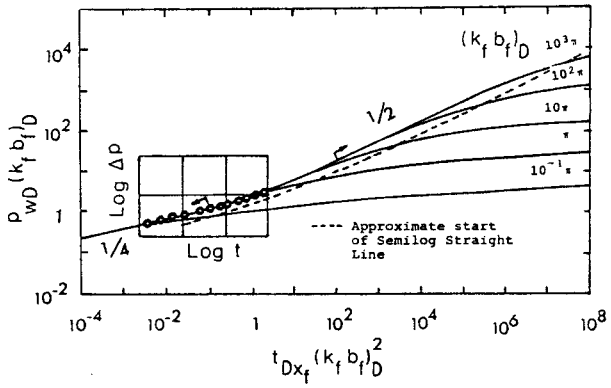

Fig. 12 – Type-curve matching for data in bilinear and transitional flow.

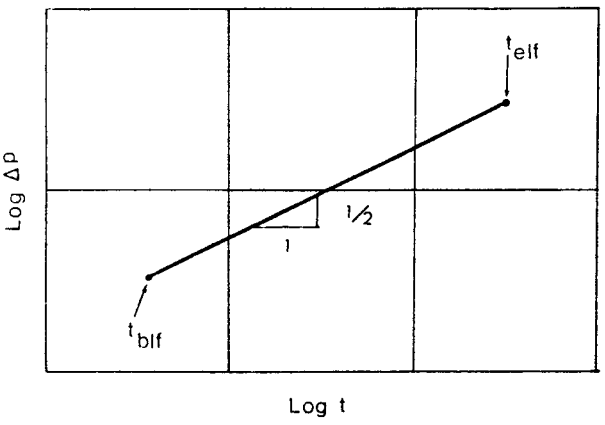

Fig. 13 – Pressure data for a half-slope straight line in a log-log graph.

Beginning of Semilog Straight Line.

$(t_{bssl})_M$

These results can be obtained if a large span of pressure data is available. It should be kept in mind that specific analysis graphs must be used for different flow regimes to obtain a better estimate of both fracture and reservoir parameters.

Now we discuss cases where all pressure data fall on a very small portion of the type curve and a complete set of information may not be obtained.

Case 1. *Pressure data exhibit one-fourth slope on a log-log graph (Fig. 7).* According to the discussion in the previous section, these data correspond to the bilinear flow period and a unique match with Fig. 10 cannot be attained. The *bilinear flow* type of analysis is the *only method available* for this case to obtain information regarding the fracture characteristics $(k_f b_f)$.

A minimum value for fracture half-length, x_f, can be estimated from Eqs. 14a through 14c for the end of the bilinear flow; that is, for $(k_f b_f)_D \geq 3$, we have

$$x_f \geq \sqrt[4]{\frac{10\beta(k_f b_f)^2 t_{ebf}}{\phi\mu c_t k}}. \quad \ldots\ldots\ldots\ldots\ldots\ldots (31)$$

Generally, wellbore storage affects a test at early time; thus, it is expected to have pressure data distorted by this effect, causing deviation from the one-fourth slope characteristic of this flow period. Fig. 11 may be applied to analyze pressure data for this case even if the duration of the test is not enough to reach the one-fourth slope portion. It is important to note that pressure behavior in Fig. 11 for both wellbore-storage-dominated and bilinear-flow portions is given by a single curve that completely eliminates the uniqueness matching problem. The correlating parameters $F_1(p_{wD})$ and $F_2(t_{Dx_f})$ used in this figure are derived in Appendix C and defined in Fig. 11.

The end of wellbore storage effects in Fig. 11 occurs when $F_2(t_{Dx_f}) \approx 2\times 10^2$; that yields

$$t_{ews} \simeq \frac{17.25}{\beta}\sqrt[3]{\frac{C^4}{(k_f b_f)^2 h^4 \phi c_t k}}. \quad \ldots\ldots\ldots\ldots (32)$$

From observation of the results presented in Fig. 11, we can see that the end of wellbore storage effects occurs three log cycles after the end of the unit slope.

This criterion is useful to determine whether the proper straight-line portion for bilinear flow analysis is chosen (see Fig. 9). If Fig. 11 is used as a type curve, the following information may be obtained: $[F_1(p_{wD})]_M$, $[F_2(t_{Dx_f})]_M$, $(\Delta p)_M$, and $(t)_M$. Hence, we can estimate the following.

Wellbore Storage Constant. For oil,

$$C = \frac{2\pi\alpha_o\beta qB\mu(t)_M}{(\Delta p)_M}\,\frac{[F_1(p_{wD})]_M}{[F_2(t_{Dx_f})]_M}, \quad \ldots\ldots (33)$$

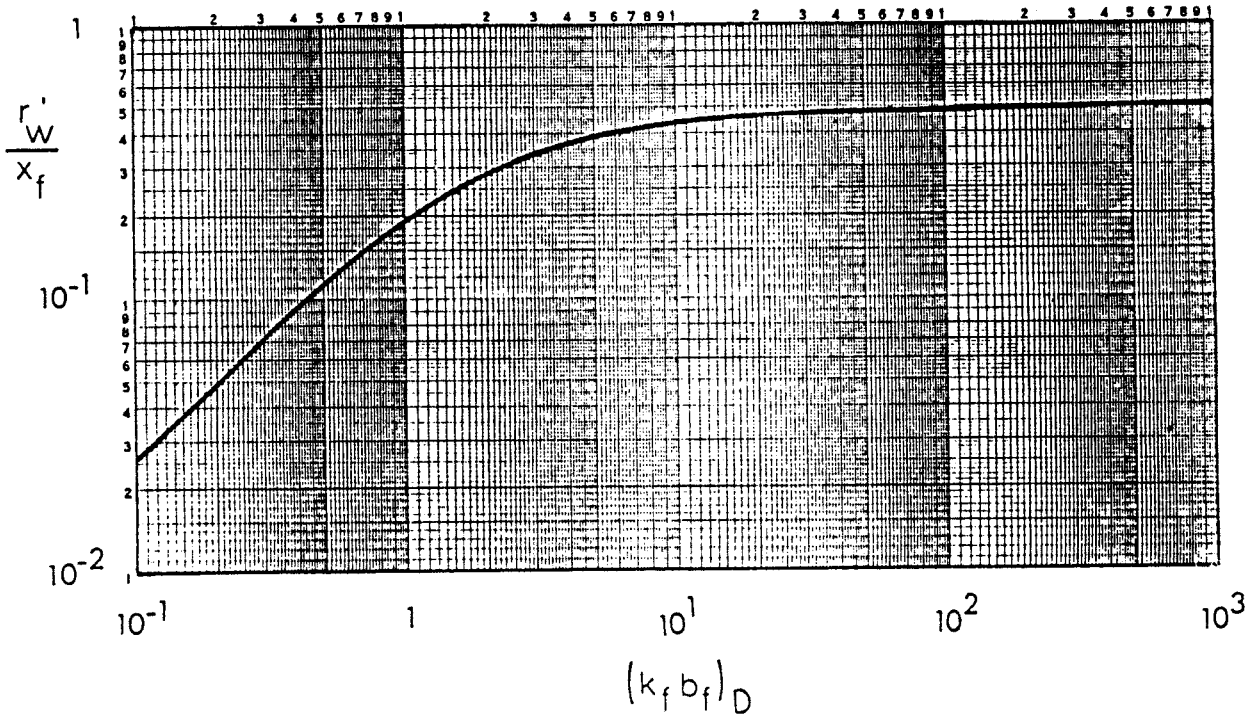

Fig. 14 – Effective wellbore radius vs. dimensionless fracture conductivity for a vertical fracture.

and, for gas,

$$C=\frac{2\pi\alpha_g\beta qT(t)_M}{[\Delta m(p)]_M}\,\frac{[F_1(p_{wD})]_M}{[F_2(t_{Dx_f})]_M}, \quad \ldots\ldots (34)$$

Fracture Conductivity. For oil,

$$k_f b_f=\frac{0.4}{h^2}\sqrt{\frac{C}{\phi c_t k}\left\{\frac{\alpha_o qB\mu[F_1(p_{wD})]_M}{(\Delta p)_M}\right\}^3}, \quad \ldots\ldots (35)$$

and, for gas,

$$k_f b_f=\frac{0.4}{h^2}\sqrt{\frac{C}{\phi c_t k}\left\{\frac{\alpha_g qT[F_1(p_{wD})]_M}{[\Delta m(p)]_M}\right\}^3}. \quad \ldots\ldots (36)$$

Case 2. *Pressure data partially match the curve for the transition period between bilinear and linear flows (Fig. 12).* In this case, the remaining portion of the data may correspond to bilinear or linear flow and the type-curve match is unique because the transition period has a characteristic shape. This comment is valid for dimensionless fracture conductivities, $(k_f b_f)_D \geq 5\pi$.

From the type-curve match of pressure data for this case in Fig. 10, we obtain $[p_{wD}(k_f b_f)_D]_M$, $[t_{Dx_f}(k_f b_f)^2_D]_M$, $(\Delta t)_M$, and $(\Delta p)_M$.
Hence, for oil,

$$\left(\frac{k_f b_f}{x_f}\right)=\frac{\alpha_o qB\mu}{h(\Delta p)_M}\left[p_{wD}(k_f b_f)_D\right]_M, \quad \ldots. (37)$$

and, for gas,

$$\left(\frac{k_f b_f}{x_f}\right)=\frac{\alpha_g qT}{h[\Delta m(p)]_M}\left[p_{wD}(k_f b_f)_D\right]_M, \quad . (38)$$

Fracture half-length and fracture conductivity. For oil or gas,

$$x_f=\left(\frac{k_f b_f}{x_f}\right)\sqrt{\frac{\beta(t)_M}{\phi\mu c_t k[t_{Dx_f}(k_f b_f)^2_D]_M}}, \quad \ldots. (39)$$

and

$$k_f b_f=(x_f)\left(\frac{k_f b_f}{x_f}\right). \quad \ldots\ldots (40)$$

Since the formation permeability generally is known from prefracture tests, the dimensionless fracture conductivity can be estimated by using results from Eq. 37 or Eq. 38. Some of these results also can be obtained from a specific analysis method corresponding to the flow period exhibited by data other than the transition flow region (i.e., bilinear flow or linear formation flow, as discussed in the bilinear flow analysis section and in Ref. 14).

If all pressure data fall on the transition period of the curve, type-curve matching (Fig. 10) is the only analysis method available.

Case 3. *Pressure data exhibit a half-slope line on a log-log graph. (Fig. 13).* For this case there is no unique match with Fig. 10; however, the linear flow

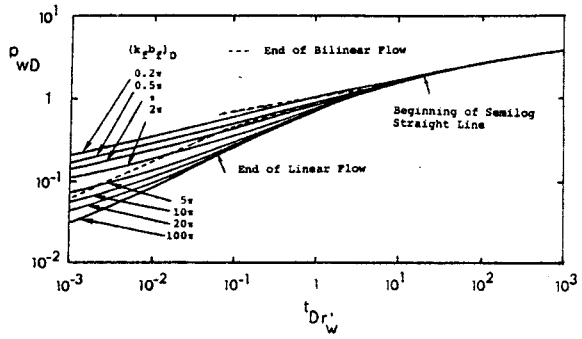

Fig. 15 – Type curve for a finite-conductivity vertical fracture.

analysis presented by Clark[14] can be applied to obtain fracture half-length if formation permeability is known. In addition, a minimum value for the dimensionless fracture conductivity, $(k_f b_f)_D$, can be estimated using Eq. 26. Note that t_{blf} in Fig. 13 represents a maximum value for the time of the beginning of the linear flow period and t_{elf} represents a minimum value for the time of the end of the half slope.

If wellbore storage effects are present at early times in a test for this case, the analysis can be made using the type curve presented by Ramey and Gringarten.[21]

Case 4. *Pressure data partially match the curve for the pseudoradial flow period.* If a large span of pressure data is not available, a unique match would not be obtained by using Fig. 10 because curves for different values of fracture conductivity are similarly shaped for the pseudoradial flow period. However, the transient pressure behavior shown in Fig. 10 can be correlated to analyze these cases better.

For the pseudoradial flow period, a fractured well behaves like an unfractured well with an effective wellbore radius being a function of dimensionless fracture conductivity, $(k_f b_f)_D$. Fig. 14 presents a graph of dimensionless effective wellbore radius, r'_w/x_f, vs. dimensionless fracture conductivity, $(k_f b_f)_D$. Notice that for large values of $(k_f b_f)_D (>300)$, the dimensionless effective wellbore radius is 0.5, as mentioned by Prats *et al.*[8]

If the dimensionless time is defined by using r'_w instead of x_f, a graph of p_{wD} vs. $t_{Dr'_w}$ provides a single curve for the pseudoradial flow period for all values of dimensionless fracture conductivity (see Fig. 15). This curve provides an excellent tool for type-curve analysis of pressure data partially falling in the pseudoradial flow period because the remaining data must follow one of the curves for different fracture conductivities. Fig. 14 must be used as an auxiliary curve to determine $(k_f b_f)_D$ when using Fig. 15.

Application of Fig. 15 to match pressure data provides $(p_{wD})_M$, $(t_{Dr_w})_M$, $(\Delta p)_M$, $(t)_M$, and $[(k_f b_f)_D]_M$. Hence, the following equations are given.

Reservoir Permeability. For oil,

$$k = \frac{\alpha_o q B \mu}{h(\Delta p)_M}(p_{wD})_M, \quad \ldots\ldots\ldots\ldots\ldots\ldots (41)$$

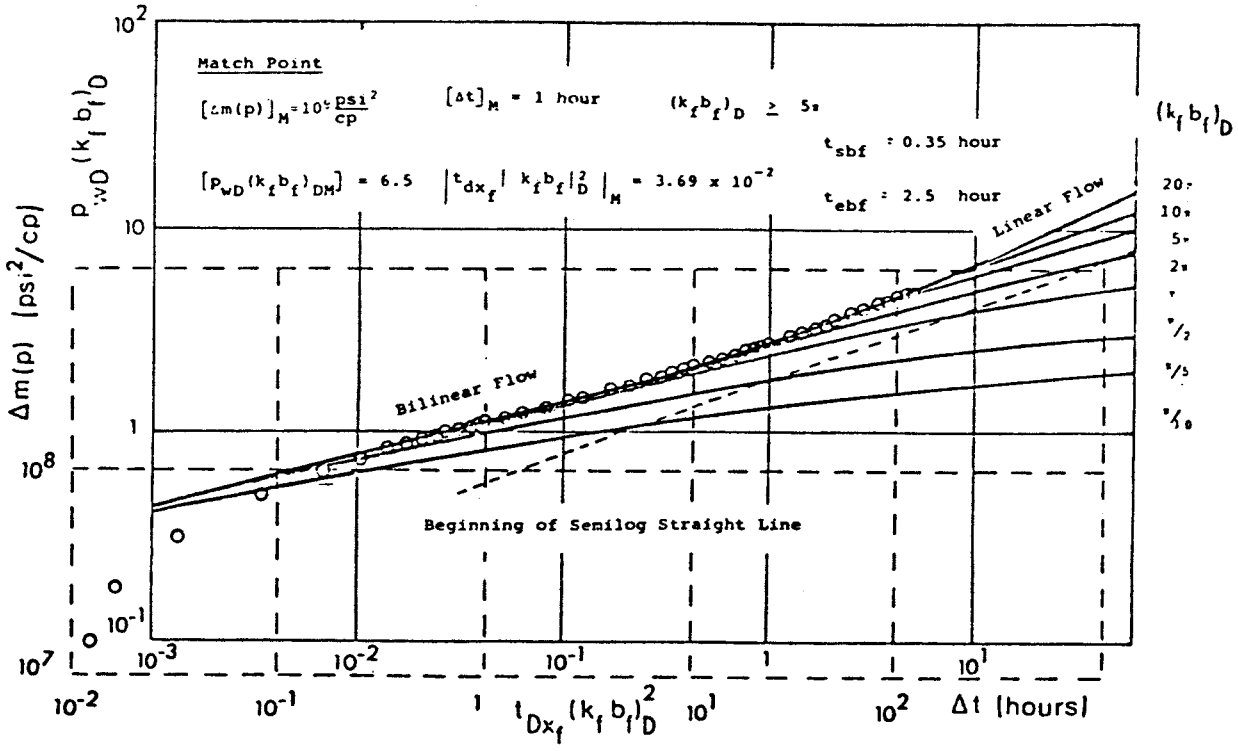

Fig. 16 – Type-curve matching for Well A.

and, for gas,

$$k=\frac{\alpha_g qT}{h[\Delta m(p)]_M}(p_{wD})_M. \quad \ldots\ldots\ldots\ldots (42)$$

Effective Wellbore Radius. For oil or gas,

$$r'_w=\sqrt{\frac{\beta k(t)_M}{\phi\mu c_t (t_{Dr'_w})_M}}. \quad \ldots\ldots\ldots\ldots\ldots (43)$$

By using $[(k_f b_f)_D]_M$ in Fig. 14, we obtain $(r'_w/x_f)_{\text{Fig. 14}}$; hence,

$$x_f=\frac{r'_w}{[r'_w/x_f]_{\text{Fig. 14}}}. \quad \ldots\ldots\ldots\ldots\ldots (44)$$

The pressure data falling in the pseudoradial flow period also must be analyzed using the semilog methods to estimate k and r'_w.

The discussion in this section clearly indicates (as mentioned by Agarwal *et al.*[29]) that caution and diligence should be exercised when applying the type-curve matching technique. To perform the type of analysis presented in the four cases, it is necessary to have prefracture information.

It should be kept in mind that application of the type-curve analysis method to pressure buildup tests is appropriate when the producing time is large.

Examples of Application

Three examples illustrate the application of several of the methods and theory previously discussed.

Well A

A buildup test was conducted in this fractured well producing in a low-permeability reservoir. Table 2 presents the information and results of the analysis for this test. Fig. 16 shows a log-log graph of pressure data matching the type curve given in Fig. 10. Notice that the first data points are influenced by wellbore storage and the rest of the data fall in both the bilinear and the transition flow periods. The match-point results also are presented in Fig. 16. A minimum value for $(k_f b_f)_D$ can be estimated from the position of the last data point with respect to the type curves; for this case, $(k_f b_f)_D$ min $\approx 5\pi$.

The end of wellbore storage occurs at approximately 0.35 hour and the end of bilinear flow is at 2.5 hours. We also see that the formation linear flow period was not reached in this test.

Since the test was not long enough to match a curve for a specific value of $(k_f b_f)_D$, this example corresponds to Case 2 in the type-curve-analysis section.

Using the pressure data match and Eq. 38, we obtain

$$\frac{k_f b_f}{x_f}=\frac{1{,}424\times 7{,}350\times 690\times 6.5}{118\times 10^9}$$

$$=0.3978 \text{ md-ft/ft}.$$

TABLE 2 – TEST INFORMATION AND ANALYSIS RESULTS FOR WELL A

Reservoir Data	
Production rate q, Mscf/D	7,350
Producing time t_p, hours	2,640
Formation thickness h, ft	118
Porosity ϕ, fraction	0.1
Permeability k, md	0.025
Formation temperature T, °R	690
Average gas viscosity μ, cp	0.0252
Total compressibility c_t, psi^{-1}	0.129×10^{-3}
Flowing wellbore pressure p_{wf}, psia	1,320

Analysis Results	Type-Curve Analysis	Bilinear Flow Analysis
$k_f b_f$, md-ft	148	154
x_f, ft	373	368
$\left(\frac{k_f b_f}{x_f}\right)$, md-ft/ft	0.3978	0.4185
$(k_f b_f)_D$	15.9	~16.71
r'_w, ft	171.6	~169.3

From the time-match information and Eq. 39, we can calculate

$$x_f=0.3978\cdot\sqrt{\frac{2.637\times 10^{-4}\times 1}{0.1\times 0.025\times 1.29\times 10^{-4}\times 0.025\times 3.69\times 10^{-2}}}$$

$$=373 \text{ ft}.$$

Now, application of Eq. 40 yields

$$k_f b_f=0.3978\times 373=148 \text{ md-ft}.$$

We also can estimate

$$(k_f b_f)_D=\frac{k_f b_f}{x_f}\frac{1}{k}$$

$$=\frac{0.3978}{0.025}=15.9.$$

From Fig. 14, $r'_w/x_f=0.46$.

$$\therefore\ r'_w=373\times 0.46=171.6 \text{ ft}.$$

Fig. 17 shows the bilinear flow graph [$\Delta m(p)$ vs. $\Delta t^{1/4}$] for this example. Based on the information provided by Fig. 16, the correct straight line is drawn. The slope of this line is 1.62×10^8 psi^2/cp-hr$^{1/4}$, and at the end of bilinear flow $\Delta m(p)_{ebf}\approx 2.05\times 10^8$ psi^2/cp-hr$^{1/4}$. Notice that the pressure curve after the end of the bilinear flow period is concave upward, indicating that $(k_f b_f)_D > 1.6$.

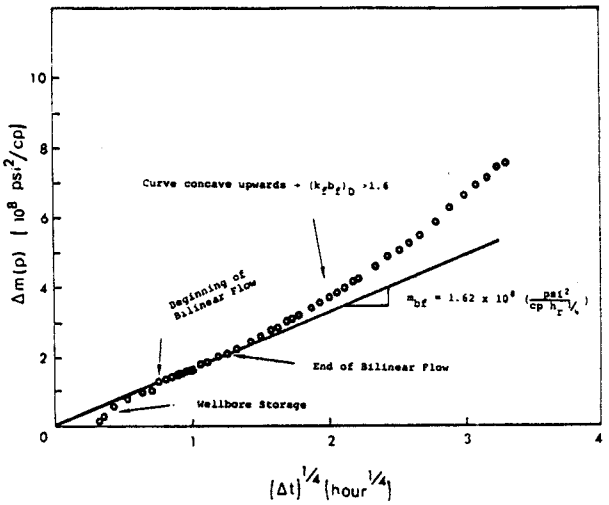

Fig. 17 – Bilinear flow graph for Well A.

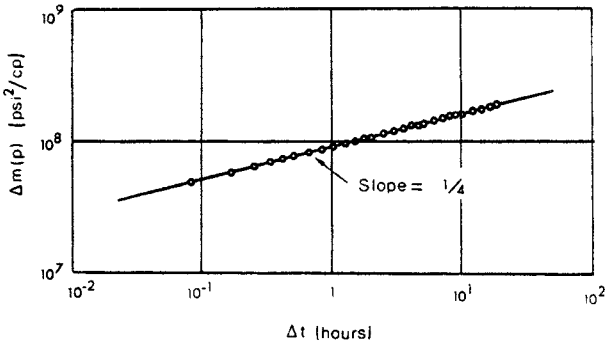

Fig. 18 – Log-log graph of pressure data for Well B.

TABLE 3 – TEST INFORMATION AND ANALYSIS RESULTS FOR WELL B

Reservoir Data	
Production rate q, Mscf/D	1,675
Producing time t_p, hours	1,800
Formation thickness h, ft	85
Porosity ϕ, fraction	0.11
Permeability k, md	0.0045
Formation temperature T, °R	675
Average gas viscosity μ, cp	0.025
Total compressibility c_t, psi^{-1}	0.152×10^{-3}
Flowing wellbore pressure p_{wf}, psia	1,250

Analysis Results	Type-Curve Analysis	Bilinear Flow Analysis
$k_f b_f$, md-ft	–	95.3
x_f, ft	–	≥692
$\left(\frac{k_f b_f}{x_f}\right)$, md-ft/ft	–	≤0.1377
$(k_f b_f)_D$	–	≤30.6
r'_w, ft	–	≤325

From Eq. 20,

$$(k_f b_f)^{1/2} = (444.75\times7{,}350\times690)/[1.62\times10^8\times118$$

$$\cdot(0.1\times0.0252\times1.29\times10^{-4}\times0.025)]^{1/4},$$

$$\therefore (k_f b_f) = 154 \text{ md-ft}.$$

Using Eqs. 22 and 2,

$$(k_f b_f)_D \approx \frac{1.38}{\left(\frac{0.025\times118\times2.05\times10^8}{1{,}424\times7{,}350\times690}\right)}$$

$$\approx 16.71.$$

Hence,

$$x_f \approx \frac{k_f b_f}{k(k_f b_f)_D}$$

$$= \frac{154}{0.025\times16.71} \approx 368 \text{ ft}.$$

From Fig. 14, $r'_w/x_f = 0.46$.

$$\therefore r'_w = 368\times0.46 = 169.3 \text{ ft}.$$

We see that the results obtained by using both the bilinear flow and the type-curve methods are approximately the same; this fact increases confidence in the analysis performed.

Well B

A buildup test was run after fracturing this gas well. Information about the test and results of analysis are presented in Table 3. A log-log graph of pressure data (Fig. 18) indicates that the test was completely dominated by bilinear flow (quarter slope), corresponding this example to Case 1 in the type-curve-analysis section.

The bilinear flow graph (Fig. 19) yields a straight line whose slope, m_{bf}, can be used to calculate $(k_f b_f)$ using Eq. 20:

$$(k_f b_f)^{1/2} = \left(444.75\times1{,}675\times675\right)/\left[0.92\times10^8\right.$$

$$\times85\times(0.11\times0.025\times1.52\times10^{-4}$$

$$\left.\times0.0045)^{1/4}\right],$$

or

$$k_f b_f = 95.3 \text{ md-ft}.$$

If we assume that the last data point corresponds to

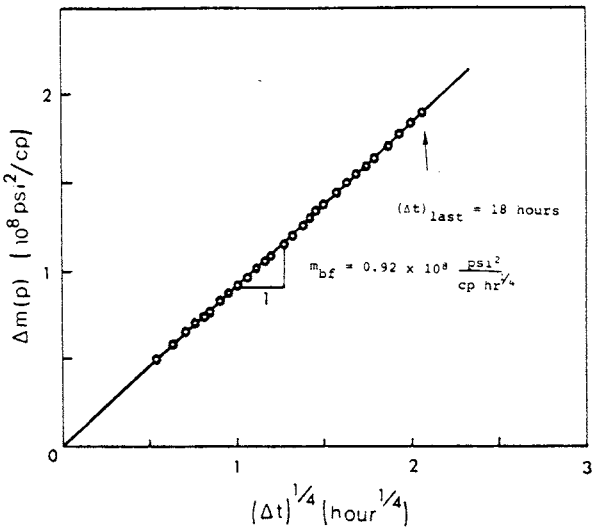

Fig. 19 – Bilinear flow graph for Well B.

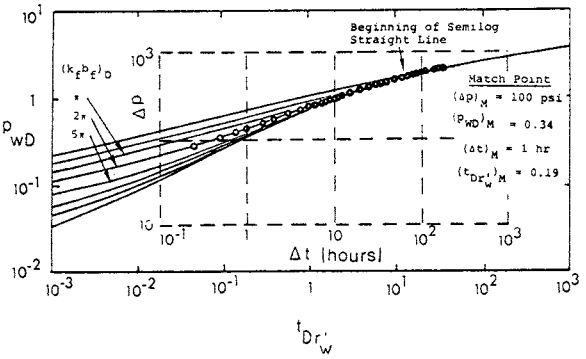

Fig. 20 – Type-curve matching for Well C.

the end of the bilinear flow period and $(k_f b_f)_D \geq 3$, then from Eq. 31,

$$x_f \geq \sqrt[4]{\frac{10 \times 2.637 \times 10^{-4} \times (95.3)^2 \times 18}{0.11 \times 0.025 \times 1.52 \times 10^{-4} \times 0.0045}}$$

$$= 692 \text{ ft},$$

and

$$\frac{k_f b_f}{x_f} \leq \frac{95.3}{692} = 0.1377 \text{ md-ft/ft}.$$

From Eq. 6,

$$(k_f b_f)_D = \left(\frac{k_f b_f}{k x_f}\right) \leq \frac{95.3}{0.0045 \times 692},$$

$$\therefore (k_f b_f)_D \leq 30.6.$$

From Fig. 14, $r'_w/x_f \leq 0.47$; hence, $r'_w \leq 0.47 \times 692$, $r'_w \leq 325$ ft.

Well C

After a flowing time of 1,890 hours, a buildup test was run on this fractured oil well. Information for the test and analysis results are presented in Table 4. Fig. 20 shows a log-log graph of the pressure data; from this graph we can see that neither a one-fourth slope nor a half slope is exhibited by the data. This figure also shows that pressure data match the curve for $(k_f b_f)_D = 2\pi$ given in Fig. 15 and the last six points fall on the semilog straight line.

From the pressure match obtained in Fig. 20 and Eq. 41, we estimate

$$k = \frac{141.2 \times 220 \times 1.2 \times 0.8 \times 0.34}{49 \times 100}$$

$$= 2.07 \text{ md}.$$

TABLE 4 – TEST INFORMATION AND ANALYSIS RESULTS FOR WELL C

Reservoir Data	
Production rate q, STB/D	220
Producing time t_p, hours	1,890
Formation thickness h, ft	49
Porosity ϕ, fraction	0.15
Viscosity μ, cp	0.8
Total compressibility c_t, psi^{-1}	17.6×10^{-6}
Formation volume factor B_o, bbl/STB	1.2
Wellbore radius r_w, ft	0.25
Flowing wellbore pressure p_{wf}, psia	1,704

Analysis Results	Type-Curve Analysis	Semilog Analysis
k, md	2.07	2.28
$(k_f b_f)_D$	2π	–
x_f, ft	88.7	–
$k_f b_f$, md-ft	1,156	–
r'_w, ft	36.89	30.37
S	– 4.99	– 4.8

Using information from the time match in Eq. 43,

$$r'_w = \sqrt{\frac{2.637 \times 10^{-4} \times 2.07 \times 1}{0.15 \times 0.8 \times 17.6 \times 10^{-6} \times 0.19}}$$

$$= 36.9 \text{ ft}.$$

From Fig. 14, $r'_w/x_f = 0.415$; hence,

$$x_f = \frac{36.9}{0.415} = 88.9 \text{ ft}.$$

The skin factor is estimated by

$$s = \ln \frac{r_w}{r'_w} = \ln \frac{0.25}{36.9} = -4.99.$$

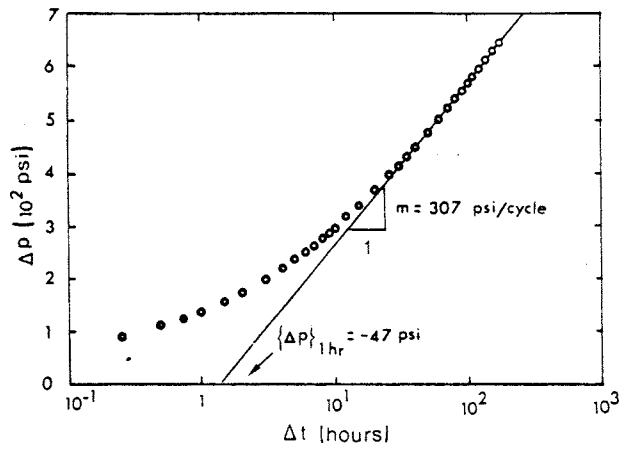

Fig. 21 – Semilog graph for Well C.

The fracture conductivity is

$$k_f b_f = (k_f b_f)_D k x_f$$

$$= 2\pi \times 2.07 \times 88.9 = 1{,}156.2 \text{ md-ft.}$$

Fig. 21 is a semilog graph for this example. The correct semilog straight line has a slope $m = 307$ psi/cycle and $(\Delta p)_{1\text{hr}} = -47$ psi. The formation permeability can be calculated as

$$k = \frac{162.6\, qB\mu}{mh}$$

$$= \frac{162.6 \times 220 \times 1.2 \times 0.8}{307 \times 49} = 2.28 \text{ md.}$$

The skin factor is

$$s = 1.151\left[\frac{(\Delta p)_{1\text{hr}}}{m} - \log\left(\frac{k}{\phi \mu c_t r_w^2}\right) + 3.2275\right]$$

$$= 1.151\left[\frac{-47}{307}\right.$$

$$\left. - \log \frac{2.28}{0.15 \times 0.8 \times 17.6 \times 10^{-6} \times (0.25)^2} + 3.2275\right] = -4.8.$$

Finally, the effective wellbore radius is

$$r'_w = r_w e^{-s} = 0.25\, e^{4.8}$$

$$= 30.37 \text{ ft.}$$

The results provided by both the type-curve analysis and semilog analysis methods are in good agreement. From these examples it is demonstrated that type-curve analysis, when applied properly, provides an excellent diagnostic tool and a technique to estimate both reservoir and fracture parameters.

Conclusions

Based on the material presented in this work, the following remarks are pertinent.

1. The transient flow behavior of a vertically fractured well may exhibit four flow periods: (a) fracture linear flow, (b) bilinear flow, (c) formation linear flow, and (d) pseudoradial flow. Bilinear flow is a new type of flow that has not been considered before.
2. A new technique is presented to analyze data in the bilinear flow period. It is shown that, during this flow period, a graph of p_{wf}[or $m(p_{wf})$] vs. $\sqrt[4]{t}$ yields a straight line whose slope is inversely proportional to $h_f (k_f b_f)^{1/2}$.
3. New type curves are now available for pressure analysis of fractured wells. The uniqueness problem in the analysis is reduced considerably with the use of these type curves.
4. Prefracture information about the reservoir is necessary to estimate fracture parameters.
5. The type-curve analysis method must be used simultaneously with the specific analysis methods (p_{wf} vs. $\sqrt[4]{t}$, p_{wf} vs. $\sqrt{t}$, and p_{wf} vs. log t) to produce reliable results.

Acknowledgments

Part of this work was developed at Stanford U. and the Inst. Mexicano del Petroleo. We are grateful to many people, especially H.J. Ramey Jr. for his encouragement and helpful comments.

Nomenclature

b_f = fracture width
B = formation volume factor
c = compressibility
C = wellbore storage coefficient
F_1, F_2 = correlating parameters for wellbore storage
h = formation thickness
h_f = fracture height
k = permeability
$k_f b_f$ = fracture conductivity
$(k_f b_f)_D$ = dimensionless fracture conductivity
m = slope of semilog straight line, gas pseudopressure
m_{bf} = slope of straight line for bilinear flow
p = pressure
q = well flow rate
r_w = wellbore radius
r'_w = effective wellbore radius
s = skin factor or Laplace space variable
t = time
Δt = shut-in time
T = reservoir temperature
x, y = space coordinates
x_f = fracture half-length
α, β = unit conversion constants
Γ = gamma function
η = hydraulic diffusivity
ϕ = porosity
μ = fluid viscosity

Subscripts

b = beginning
bf = bilinear flow
g = gas
D = dimensionless
e = end
f = fracture, flowing
i = initial
lf = linear flow
o = oil
t = total
x_f = based on x_f
w = wellbore

References

1. Matthews, C.S. and Russell, D.G.: *Pressure Buildup and Flow Tests in Wells*, Monograph Series, SPE, Dallas (1967) 1.
2. Ramey, H.J. Jr., Kumar, A., and Gulati, M.S.: *Gas Well Test Analysis Under Water-Drive Conditions*, AGA, Arlington, VA (1973).
3. Earlougher, R.C. Jr.: *Advances in Well Test Analysis*, Monograph Series, SPE, Dallas (1977) 5.
4. *Theory and Practice of Testing of Gas Wells*, third edition, Energy Resources Conservation Board, Calgary, Alta. (1975).
5. Ramey, H.J. Jr.: "Practical Use of Modern Well Test Analysis," paper SPE 5878 presented at the SPE 46th Annual California Regional Meeting, Long Beach, April 8-9, 1976.
6. Raghavan, R.: "Pressure Behavior of Wells Intercepting Fractures," *Proc.*, Invitational Well-Testing Symposium, Berkeley, CA, Oct. 19-21, 1977.
7. Dyes, A.B., Kemp, C.E., and Caudle, B.H.: "Effect of Fractures on Sweep-Out Patterns," *Trans.*, AIME (1958) **213**, 245.
8. Prats, M., Hazebroek, P., and Stickler, W.R.: "Effect of Vertical Fractures on Reservoir Behavior – Compressible-Fluid Case," *Soc. Pet. Eng. J.* (June 1962) 87-94; *Trans.*, AIME, **225**.
9. Scott, J.O.: "The Effect of Vertical Fractures on Transient Pressure Behavior of Wells," *J. Pet. Tech.* (Dec. 1963) 1365-1369; *Trans.*, AIME, **228**.
10. Horner, D.R.: "Pressure Build-Up in Wells," *Proc.*, Third World Pet. Cong., The Hague (1951) Sec. II, 503-523.
11. Miller, C.C., Dyes, A.V., and Hutchinson, C.A. Jr.: "Estimation of Permeability and Reservoir Pressure from Bottom-Hole Pressure Build-Up Characteristics," *Trans.*, AIME (1950) **189**, 91-104.
12. Matthews, C.S., Brons, F., and Hazebroek, P.: "A Method for Determination of Average Pressure in a Bounded Reservoir," *Trans.*, AIME (1954) **201**, 182-191.
13. Russell, D.G. and Truitt, N.E.: "Transient Pressure Behavior in Vertically Fractured Reservoirs," *J. Pet. Tech.* (Oct. 1964) 1159-1170; *Trans.*, AIME, **231**.
14. Clark, K.K.: "Transient Pressure Testing of Fractured Water Injection Wells," *J. Pet. Tech.* (June 1968) 639-643; *Trans.*, AIME, **243**.
15. Millheim, K.K. and Cichowicz, L.: "Testing and Analyzing Low-Permeability Fractured Gas Wells," *J. Pet. Tech.* (Feb. 1968) 193-198; *Trans.*, AIME, **243**.
16. Raghavan, R., Cady, G.V., and Ramey, H.J. Jr.: "Well-Test Analysis for Vertically Fractured Wells," *J. Pet. Tech.* (Aug. 1972) 1014-1020; *Trans.*, AIME, **253**.
17. Gringarten, A.C. and Ramey, H.J. Jr.: "Unsteady-State Pressure Distributions Created by a Well With a Single Infinite-Conductivity Vertical Fracture, *Soc. Pet. Eng. J.* (Aug. 1974) 347-360; *Trans.*, AIME, **257**.
18. Gringarten, A.C. and Ramey, H.J. Jr.: "Unsteady-State Pressure Distributions Created by a Well With a Single Horizontal Fracture, Partial Penetration or Restricted Entry," *Soc. Pet. Eng. J.* (Aug. 1974) 413-426; *Trans.*, AIME, **257**.
19. Gringarten, A.C., Ramey, H.J. Jr., and Raghavan, R.: "Applied Pressure Analysis for Fractured Wells," *J. Pet. Tech.* (July 1975) 887-892; *Trans.*, AIME, **259**.
20. Wattenbarger, R.A. and Ramey, H.J. Jr.: "Well Test Interpretations of Vertically Fractured Gas Wells," *J. Pet. Tech.* (May 1969) 625-632; *Trans.*, AIME, **246**.
21. Ramey, H.J. Jr. and Gringarten, A.C.: "Effect of High-Volume Vertical Fractures on Geothermal Steam Well Behavior," *Proc.*, Second United Nations Symposium on the Use and Development of Geothermal Energy, San Francisco, May 20-29, 1975.
22. Cinco, H., Ramey, H.J. Jr., and Miller, F.: "Unsteady-State Pressure Distribution Created by a Well With an Inclined Fracture," paper SPE 5591 presented at the SPE 50th Annual Technical Conference and Exhibition, Dallas, Sept. 30-Oct. 3, 1975.
23. Raghavan, R. and Hadinoto, N.: "Analysis of Pressure Data for Fractured Wells: The Constant-Pressure Outer Boundary," *Soc. Pet. Eng. J.* (April 1978) 139-150; *Trans.*, AIME, **265**.
24. Raghavan, R., Uraiet, A., and Thomas, G.W.: "Vertical Fracture Height: Effect on Transient Flow Behavior," *Soc. Pet. Eng. J.* (Aug. 1978) 265-277.
25. Cinco, H., Samaniego, F., and Domínguez, N.: "Transient Pressure Behavior for a Well with a Finite-Conductivity Vertical Fracture," *Soc. Pet. Eng. J.* (Aug. 1978) 253-264.
26. Holditch, S.A. and Morse, R.A.: "The Effects of Non-Darcy Flow on the Behavior of Hydraulically Fractured Wells," *J. Pet. Tech.* (Oct. 1976) 1169-1178.
27. Ramey, H.J. Jr., Barker, B., Arihara, N., Mao, M.L., and Marques, J.K.: "Pressure Transient Testing of Hydraulically Fractured Wells," paper presented at American Society Topical Meeting, Golden, CO, April 12-14, 1977.
28. Cinco, H. and Samaniego, F.: "Effect of Wellbore Storage and Damage on the Transient Pressure Behavior of Vertically Fractured Wells," paper SPE 6752 presented at the SPE 52nd Annual Technical Conference and Exhibition, Denver, Oct. 9-12, 1977.
29. Agarwal, R.G., Carter, R.D., and Pollock, C.B.: "Evaluation and Prediction of Performance of Low-Permeability Gas Wells Stimulated by Massive Hydraulic Fracturing," *J. Pet. Tech.* (March 1979) 362-372; *Trans.*, AIME, **267**.
30. Barker, B.: "Transient Flow to Finite-Conductivity Vertical Fractures," PhD dissertation, Stanford U., Palo Alto, CA 1977.
31. Barker, B.J. and Ramey, H.J. Jr.: "Transient Flow to Finite-Conductivity Vertical Fractures," paper SPE 7489 presented at the SPE 53rd Annual Technical Conference and Exhibition, Houston, Oct. 1-3, 1978.
32. Scott, J.O.: "A New Method for Determining Flow Characteristics of Fractured Wells – Application to Gas Wells in Tight Formations," paper 78-T-2, AGA 1978 Transmission Conference, Montreal, T-279-186.

APPENDIX A
Short-Time Transient Pressure Behavior for a Well With a Finite-Conductivity Fracture

Derivation of Solution

Let us consider the system described in the text of this paper. A fractured well produces at a constant flow rate from an infinite reservoir. At small time values, the pressure behavior of the system is not affected by the tips of the fracture. In addition, the flow in the formation is essentially linear and perpendicular to the fracture plane. The reservoir and the fracture may be treated as two different homogeneous regions.[25]

If the flow within the fracture is assumed to be linear, the pressure behavior can be described by

$$\frac{\partial^2 p_{fD}}{\partial x_D^2} + \frac{2}{(k_f b_f)_D} \frac{\partial p_D}{\partial y_D}\bigg|_{y_D=0}$$

$$= \frac{1}{\eta_{fD}} \frac{\partial p_{fD}}{\partial t_{Dx_f}} \quad \ldots\ldots\ldots\ldots\ldots\ldots (A\text{-}1)$$

for $0 < x_D < \infty$, $t_{Dx_f} > 0$.

Initial Condition.

$$p_{fD} = 0,\ t_{Dx_f} = 0,\ 0 \le x_D < \infty. \quad \ldots\ldots\ldots\ldots (A\text{-}2)$$

Boundary Conditions.

$$\left.\frac{\partial p_{fD}}{\partial x_D}\right|_{x_D=0} = -\frac{\pi}{(k_f b_f)_D},\ t_{Dx_f} > 0, \quad \ldots\ldots\ldots\ldots\ldots\ldots (A\text{-}3)$$

and

$$\lim_{x_D \to \infty} p_{fD} = 0,\ t_{Dx_f} > 0, \quad \ldots\ldots\ldots\ldots\ldots\ldots (A\text{-}4)$$

where, in oilfield units,

$$p_{fD} = \frac{kh[p_i - p_f]}{141.2\, qB\mu},$$

$$p_D = \frac{kh[p_i - p]}{141.2\, qB\mu},$$

$$t_{Dx_f} = \frac{0.000264\, kt}{\phi\mu c_t x_f^2},$$

$$x_D = \frac{x}{x_f},$$

and

$$y_D = \frac{y}{x_f}.$$

The variables not included above are defined in the text. p and p_f represent the formation pressure and the fracture pressure, respectively, x is the flow direction in the fracture, and y is the formation flow direction perpendicular to the fracture plane.

The transient flow in the formation may be described by

$$\frac{\partial^2 p_D}{\partial y_D^2} = \frac{\partial p_D}{\partial t_{Dx_f}};\ 0 < y_D < \infty;$$

$$t_{Dx_f} > 0. \quad \ldots\ldots\ldots\ldots\ldots\ldots (A\text{-}5)$$

Initial Condition.

$$p_D = 0;\ 0 < y_D < \infty;\ t_{Dx_f} = 0. \quad \ldots\ldots\ldots\ldots (A\text{-}6)$$

Boundary Conditions.

$$p_D\big|_{y_D=0} = p_{fD};\ t_{Dx_f} > 0, \quad \ldots\ldots\ldots\ldots (A\text{-}7)$$

and

$$\lim_{y_D \to \infty} p_D = 0;\ t_{Dx_f} > 0. \quad \ldots\ldots\ldots\ldots\ldots (A\text{-}8)$$

The two partial differential equations are already coupled by the boundary conditions. Application of the Laplace transformation with respect to time to Eqs. A-1 through A-8 and simplification yields

$$\frac{\partial^2 \bar{p}_{fD}}{\partial x_D^2} + \frac{2}{(k_f b_f)_D} \left.\frac{\partial \bar{p}_D}{\partial y_D}\right|_{y_d=0}$$

$$= \frac{s}{\eta_{fD}} \bar{p}_{fD};\ 0 < x_D < \infty. \quad \ldots\ldots\ldots (A\text{-}9)$$

Boundary Conditions.

$$\left.\frac{\partial \bar{p}_{fD}}{\partial x_D}\right|_{x_d=0} = -\frac{\pi}{(k_f b_f)_D}, \quad \ldots\ldots\ldots\ldots (A\text{-}10)$$

$$\lim_{x_D \to \infty} \bar{p}_{fD} = 0, \quad \ldots\ldots\ldots\ldots\ldots\ldots (A\text{-}11)$$

and

$$\frac{\partial^2 \bar{p}_D}{\partial y_D^2} = s\bar{p}_D;\ 0 < y_D < \infty. \quad \ldots\ldots\ldots\ldots (A\text{-}12)$$

Boundary Conditions.

$$\bar{p}_D\big|_{y_D=0} = \bar{p}_{fD}, \quad \ldots\ldots\ldots\ldots\ldots\ldots (A\text{-}13)$$

$$\lim_{y_D \to \infty} \bar{p}_D = 0, \quad \ldots\ldots\ldots\ldots\ldots\ldots (A\text{-}14)$$

where

$$\bar{p}_{fD}(x_D, s) = \mathcal{L}_{t_{Dx_f}}[p_{fD}(x_D, t_{Dx_f})],$$

and

$$\bar{p}_D(y_D, s) = \mathcal{L}_{t_{Dx_f}}[p_D(y_D, t_{Dx_f})].$$

Now let us define

$$\bar{\bar{p}}_D(r,s) = \mathcal{L}_{y_D}[\bar{p}_D(y_D, s)].$$

Application of the Laplace transformation, with respect to y_D, to Eq. A-12 yields

$$r^2 \bar{\bar{p}}_D - r p_D\big|_{y_D=0} - \left.\frac{\partial \bar{p}_D}{\partial y_D}\right|_{y_D=0} = s\bar{\bar{p}}_D. \quad \ldots (A\text{-}15)$$

By solving for $\bar{\bar{p}}_D$ and considering Eq. A-13, we obtain

$$\bar{\bar{p}}_D = \frac{r\bar{p}_{fD} + \left.\frac{\partial p_D}{\partial y_D}\right|_{y_D=0}}{r^2 - s}. \quad \ldots\ldots\ldots (A\text{-}16)$$

The inversion of this equation with respect to y_D yields

$$\bar{p}_D = \bar{p}_{fD} \cosh(\sqrt{s}\, y_D) + \left.\frac{\partial \bar{p}_D}{\partial y_D}\right|_{y_D=0}$$

$$\cdot \frac{\sinh(\sqrt{s}\, y_D)}{\sqrt{s}}. \quad \ldots\ldots\ldots\ldots\ldots (A\text{-}17)$$

From Eqs. A-14 and A-17, we can write

$$\left.\frac{\partial \bar{p}_D}{\partial y_D}\right|_{y_D=0} = -\bar{p}_{fD}\sqrt{s}. \quad \ldots\ldots\ldots\ldots (A\text{-}18)$$

Next, substitution of Eq. A-18 into Eq. A-9 allows us to write a partial differential equation with only one dependent variable:

$$\frac{\partial^2 \bar{p}_{fD}}{\partial x_D^2} = \frac{s}{\eta_{fD}} + \frac{2\sqrt{s}}{(k_f b_f)_D}\bar{p}_{fD}. \quad \ldots\ldots\ldots (A\text{-}19)$$

The solution of Eq. A-19 with boundary conditions given by Eqs. A-10 and A-11 can be expressed as

$$\bar{p}_{fD} = \frac{\pi \exp\left\{-x_D\left[\frac{s}{\eta_{fD}} + \frac{2\sqrt{s}}{(k_f b_f)_D}\right]^{1/2}\right\}}{(k_f b_f)_D\, s\left[\frac{s}{\eta_{fD}} + \frac{2\sqrt{s}}{(k_f b_f)_D}\right]^{1/2}}. \quad \ldots\ldots\ldots\ldots\ldots\ldots (A\text{-}20)$$

The pressure at the wellbore $\bar{p}_{wD}$ is calculated at $x_D = 0$; thus,

$$\bar{p}_{wD} = \frac{\pi}{(k_f b_f)_D\, s\left[\frac{s}{\eta_{fD}} + \frac{2\sqrt{s}}{(k_f b_f)_D}\right]^{1/2}}. \quad \ldots (A\text{-}21)$$

Finally, the Laplace inversion of Eq. A-21 with respect to t_{Dx_f} produces

$$p_{wD} = \frac{\sqrt{\pi \eta_{fD}}}{(k_f b_f)_D}\int_0^{t_{Dxf}} \cdot \frac{\operatorname{erfc}\left[\frac{\eta_{fD}\lambda}{(k_f b_f)_D\,(t_{Dx_f}-\lambda)^{1/2}}\right]}{\sqrt{\lambda}}\, d\lambda. \quad \ldots\ldots\ldots\ldots\ldots\ldots (A\text{-}22)$$

Unfortunately, Eq. A-22 is too complex to analyze both the short- and long-time behavior of the solution. Eq. A-21 may be used for this purpose.

Short-Time Behavior

The short-time approximation of the solution can be obtained from Eq. A-21 by taking the limit as the variable s approaches infinity. Thus,

$$\bar{p}_{wD} \simeq \frac{\pi\sqrt{\eta_{fD}}}{(k_f b_f)_D s^{3/2}}. \quad \ldots\ldots\ldots\ldots\ldots (A\text{-}23)$$

Inversion of this formula produces Eq. 8.

Long-Time Behavior

We can obtain the solution for large values of time by taking the limit of Eq. A-21 as s approaches zero; hence,

$$\bar{p}_{wD} \simeq \frac{\pi}{\sqrt{2(k_f b_f)_D}\, s^{5/4}}. \quad \ldots\ldots\ldots\ldots (A\text{-}24)$$

Inverting Eq. A-24 produces Eq. 12. This solution also may be obtained by considering incompressible flow within the fracture.

Total Formation Flow

Eqs. A-18 and A-20 can be used to calculate the fraction of the well flow rate that is being produced from the formation. The formula for this case appears to be

$$\frac{q_{\text{formation}}}{q} = 1 - \exp\left(\frac{4t_{Dx_f}}{\pi^2 C_{fDf}^2}\right) \cdot \operatorname{erfc}\left(\frac{2\sqrt{t_{Dx_f}}}{\pi C_{fDf}}\right). \quad \ldots\ldots\ldots (A\text{-}25)$$

For small values of t_{Dx_f}, the amount of fluid coming from the formation is negligible; however, at large values of t_{Dx_f}, most of the produced fluid comes from the formation. This illustrates the physical behavior of the system.

APPENDIX B

Derivation of Correlation Parameters for Bilinear and Linear Flows

If we consider a fracture of length x_f, Eq. A-4 becomes

$$\left.\frac{\partial p_{fD}}{\partial x_D}\right|_{x_D=1} = 0. \quad \ldots\ldots\ldots\ldots\ldots\ldots (B\text{-}1)$$

Using Eq. B-1 instead of Eq. A-4 and considering incompressible flow within the fracture, the Laplace transformation solution for the problem stated in Appendix A is

$$\bar{p}_{w_D} = \left(-\pi + \sum_{n=0}^{\infty} 2\pi \exp\left\{-2n \cdot \left[2\sqrt{\frac{s}{(k_f b_f)_D^2}}\right]^{1/2}\right\}\right) \Big/ \left(s(k_f b_f)_D \cdot \left[2\sqrt{\frac{s}{(k_f b_f)_D^2}}\right]^{1/2}\right), \quad \ldots\ldots\ldots\ldots (B\text{-}2)$$

or

$$\bar{p}_{w_D}(k_f b_f)_D^3 = \left(-\pi + \sum_{n=0}^{\infty} 2\pi \exp\left\{-2n \cdot \left[2\sqrt{\frac{s}{(k_f b_f)_D^2}}\right]^{1/2}\right\}\right) \Big/ \left(\frac{s}{(k_f b_f)_D^2} \cdot \left[2\sqrt{\frac{s}{(k_f b_f)_D^2}}\right]^{1/2}\right). \quad \ldots\ldots\ldots\ldots (B\text{-}3)$$

Hence,

$$\bar{p}_{w_D}(k_f b_f)_D = \frac{1}{(k_f b_f)_D^2} f\left[\frac{s}{(k_f b_f)_D^2}\right]. \quad \ldots (B\text{-}4)$$

From Laplace inversion tables,

$$p_{w_D}(k_f b_f)_D = F[t_{Dx_f} \cdot (k_f b_f)_D^2]. \quad \ldots\ldots (B\text{-}6)$$

Hence, a graph of $p_{w_D}\ (k_f b_f)_D$ vs. $t_{Dx_f}\ (k_f b_f)^2$ yields a single curve.

For small values of dimensionless time, Eq. B-3 yields Eq. A-24, corresponding to bilinear flow.

The long-time approximation of Eq. B-3 yields

$$\bar{p}_{w_D} \simeq \frac{\pi}{2s^{3/2}}, \quad \ldots\ldots\ldots\ldots\ldots\ldots\ldots\ldots \text{(B-7)}$$

which is the Laplace transform of the dimensionless pressure for the formation linear flow.

APPENDIX C
Derivation of Correlation Parameters for Bilinear Flow with Wellbore Storage Effects

When wellbore storage effects are considered in the flow problem defined in Appendix A, the boundary condition at $x_D = 0$ becomes

$$\left.\frac{\partial p_{fD}}{\partial x_D}\right|_{x_D=0} = -\frac{\pi}{(k_f b_f)_D}\left(1 - C_{Df}\frac{\partial p_{wD}}{\partial t_{Dx_f}}\right), \quad \text{(C-1)}$$

where

$$C_{Df} = \frac{C}{2\pi\phi c_t h x_f^2}, \quad \ldots\ldots\ldots\ldots\ldots\ldots \text{(C-2)}$$

and C is the wellbore storage coefficient.

If flow within the fracture is considered incompressible and Eq. C-1 is taken instead of Eq. A-3, the solution for the wellbore pressure in the Laplace space is given by

$$\bar{p}_{wD} = \frac{\pi}{\sqrt{2(k_f b_f)_D}\, s^{5/4} + \pi C_{Df} s^2}, \quad \ldots\ldots \text{(C-3)}$$

which can be written as

$$\frac{(k_f b_f)_D^{4/3}}{C_{Df}^{5/3}}\bar{p}_{wD} = \pi\left\{\sqrt{2}\left[\frac{C_{Df}^{4/3}s}{(k_f b_f)_D^{2/3}}\right]^{5/4} + \pi\left[\frac{C_{Df}^{4/3}s}{(k_f b_f)_D^{2/3}}\right]^2\right\}. \quad \ldots \text{(C-4)}$$

From properties of the Laplace transformation,

$$L^{-1}f(as) = \frac{1}{a}F\left[\frac{t}{a}\right]. \quad \ldots\ldots\ldots\ldots\ldots\ldots \text{(C-5)}$$

Hence, Eq. C-4 can be written as

$$\frac{(k_f b_f)_D^{2/3}}{(C_{Df})^{1/3}}p_{wD} = F\left[\frac{(k_f b_f)_D^{2/3}}{(C_{Df})^{4/3}}t_{Dx_f}\right]. \quad \ldots\ldots\ldots\ldots\ldots\ldots \text{(C-6)}$$

This means that the bilinear flow solutions including wellbore storage are represented by a single curve when graphed in terms of

$$\frac{(k_f b_f)_D^{2/3}}{C_{Df}^{1/3}}p_{wD} \text{ vs. } \frac{(k_f b_f)_D^{2/3}}{(C_{Df})^{4/3}}t_{Dx_f}.$$

SI Metric Conversion Factors

cp	× 1.0*	E−03	= Pa·s
ft	× 3.048*	E−01	= m
psi	× 6.894 757	E+00	= kPa

*Conversion factor is exact.

JPT

Original manuscript received in Society of Petroleum Engineers office Aug. 10, 1978. Paper accepted for publication June 4, 1979. Revised manuscript received July 6, 1981. Paper (SPE 7490) first presented at the SPE 53rd Annual Technical Conference and Exhibition, held in Houston, Oct. 1-3, 1978.